

Observations of long-period waves in the nearshore waters of central west coast of India during the fall inter-monsoon period

M.M. Amrutha, V. Sanil Kumar and Jesbin George

Ocean Engineering Division, Council of Scientific & Industrial Research-National Institute of Oceanography, Dona Paula, Goa 403 004 India

*Correspondence to Sanil Kumar: Tel: 0091 8322450327 email: sanil@nio.org

Abstract

The waves measured in the eastern Arabian Sea during the fall inter-monsoon period (October) are examined at 4 locations during 2010-2015. Multi-modal features have been observed in measured wave spectra due to independent wave systems corresponding to long-period swells generated by remote storms, swells generated by nearby storms and locally generated wind waves. In October, the long-period waves (peak wave period > 18 s) appeared 5 to 7 times in different years and the significant wave height of these long-period waves are less than 1.4 m. The spatial distribution of peak wave period based on the numerical wave model shows that the presence of long-period swells along the 350 km stretch of the eastern Arabian Sea is almost in the same day. It is observed that the high waves (significant wave height > 4 m) generated in an area bounded by $40-60^{\circ}$ S and $20-40^{\circ}$ E in the south Indian Ocean reached the measurement locations in 5-6 days and resulted in the long-period waves. Relatively high percentage of long-period waves are observed in 2011 and 2015 compared to other years due to the reduction in short-period waves at the study location due to the influence of Indian Ocean Dipole.

Keywords: Surface waves, swells, wave spectrum, significant wave height, eastern Arabian Sea

1. Introduction

The wind pattern in the Arabian Sea (AS) changes between the boreal summer and winter monsoon (Shetye et al., 1985). During the summer monsoon (June to September), the winds are much stronger and during the transition period (October), the winds are weaker and these change in the wind pattern produce a similar shift in the waves in the AS (Kumar et al., 2012; Kumar and Anjali, 2015). Hence, the wave characteristics in the eastern AS undergo changes due to the seasonal reversal of monsoon winds (Anoop et al., 2015). The seasonal variations along the eastern AS have been well characterized and shown a monsoon-non-monsoon pattern and the general variations within a year are similar (Kumar et al., 2003; Kumar et al., 2014). Studies on surface waves in the eastern AS has generally focused on the boreal summer monsoon (Kumar et al., 2000; Kumar et al., 2011; Amrutha et al., 2015) and the period before the summer monsoon (Neetu et al., 2006; Vethamony et al., 2011; Amrutha et al., 2016a). Even though the annual wave characteristics of eastern AS are studied (Glejin et al., 2013; Kumar et al., 2014; Dora and Kumar, 2015), little attention has been given to the inter-monsoon period (October), which feature a short-lived and intense upper oceanic jet in the equatorial zone of the Indian Ocean (Hastenrath et al., 1993). The annual mean of the wind field through the equatorial Indian ocean is weak and westerly in nature with a strong semi-annual westerly component during both inter-monsoons (Schott and McCreary, 2001; Schott et al., 2009). Indian Ocean Dipole (IOD), an interannual mode of variability, is a major ocean-atmosphere coupled phenomena in the equatorial Indian ocean with cooler (warmer) sea surface temperature in the eastern (western) than the seasonal climatology (Saji et al., 1999). During IOD events Sea Surface Temperature anomalies are strongly coupled to surface wind anomalies in the central equatorial Indian Ocean (Saji et al., 1999). Surface winds reverse direction from westerlies to easterlies during the peak phase of positive IOD events (Rao et al., 2002). Since the wind is the major generating force of surface waves in the Ocean, the wind anomaly caused by IOD and El Niño Southern Oscillation (ENSO) (Schott et al., 2009) induce the change in wave climate. Recently Anoop et al. (2016) examined the impact of the IOD on the surface wind field of AS and its effect on the wave climate of eastern AS and reported influence of IOD on the surface wind field and a reduction in wind-seas in October during positive IOD years. Madden-Julian Oscillation (MJO) is a dominant intra-seasonal mode of oscillations which recurs every 30-60 days propagating eastward near the equator and an important factor of active and break phases of Indian and Australian monsoons (Madden and Julian, 1971) with intraseasonal and interannual variability (Mehta and Krishnamurthi 1988) and are seasonally phase locked (e.g. Saji et al. 1999).

Swells in the ocean surface can travel thousands of kilometres (Munk et al., 1963) and the identification of low-frequency swells propagating great distances from the generation region is important in wave hindcast studies (Ardhuin et al., 2009). Over the global ocean, 75% of the time, wave conditions are dominated by the swell (Semedo et al., 2011). Partially sheltered by the Africa continent, some of the Southern Ocean westerly swells could not reach the NIO. The annual climatology of swells and wind-seas indicates that the waves in NIO are dominated by swells (Semedo et al., 2011; Anoop et al., 2015) and the contribution of swells in the observed data ranged from 46 to 60% off the central west coast of India (Kumar et al., 2014). In the eastern AS, Glejin et al. (2016) observed low-amplitude (significant wave height < 1 m) long-period swells during 1.4-3.6% of the time in a year and are mainly during the non-monsoon seasons. The long-period swells cause significant heave motions of oil drilling rigs and interfere with other offshore operations (Gjevik et al., 1988). The ports exposed to open ocean, experience a reduction in efficiency of cargo handling operations and mooring line breakages due to long-period swells and its orientation with respect to moored vessel (McComb et al., 2009). Long-period swells (peak wave period, $T_p > 15$ s) are observed in the northern AS during 2009 (Kumar et al., 2011). Off the central west coast of India, southwest waves with T_p values greater than 18 s are observed (Kumar et al., 2014). During the summer monsoon, due to the interaction of monsoonal waves (immature swells) with long-period swells, the spectral peak frequency slightly moved towards the high-frequency region (Amrutha et al., 2015). Since the eastern AS becomes calm in October (Glejin et al., 2013), during this period, the presence of long-period swells is also expected. October-November is the period during which tropical cyclone is formed in the north Indian Ocean (NIO) (Pattanaik et al., 2013).

In this paper, we examine the characteristics of waves in the eastern AS during October based on data measured off Vengurla at 15 m water depth from 2013 to 2015 and at 5 m water depth during 2014 and 2015. The measured wave data at 3 other locations in water depth 9 to 15 m covering 350 km stretch of the eastern AS during 2010 to 2015 are also used in the study. The paper is arranged as follows. Section 2 contains the details of study area along with data and methodology employed in the study. Section 3 provides a discussion of the results, and Section 4 summarizes the conclusions.

2. Study area, data and methods

2.1 Study area

The study area is the nearshore waters of the central west coast of India (Fig. 1). During the spring tide, the tidal range in the area is ~ 2.3 m and during the neap tide, it is ~ 1.3 m (Amrutha et al., 2015). The ERA-Interim reanalysis data from European Centre for Medium-Range Weather

Forecasts (ECMWF) at every 6 h interval with a spatial resolution of 0.5° during January, April, July, and October averaged over the years 2010 to 2015 is presented in Figure 2 to show the seasonal variation of winds and waves in the AS. The waves in the AS show strong seasonal variation due to the variation in the winds similar to the earlier observations (Kumar et al., 2012; Anoop et al., 2015). During the non-monsoon season, the wave climate is primarily mixed sea and swell (Dora and Kumar, 2015). During July, the monthly average wind speed in the AS reaches 14-15 m/s with the significant wave height (H_{m0}) up to 5 m (Fig. 2). The average H_{m0} in the eastern AS during July varies from 2 to 4 m and the wave height increases from south to north (Glejin et al., 2012). The average H_{m0} in the present study area is 1.8-2 m during the summer monsoon period and is 0.6-0.8 m during the remaining period with an annual average value of 1 to 1.2 m (Kumar et al., 2014). Off Vengurla, Amrutha et al. (2015) reported seasonal average H_{m0} of ~ 2 m during the summer monsoon period and 1 m as the annual average value. During October, the wind speeds reach minimum value (< 4 m/s) over entire AS (Fig. 2). At Honnavar, the wave measurement location is 2.5 km from the west coast of India and at Ratnagiri, it is 2 km. The depth contours of 20, 50 and 100 m occur at 10, 30 and 75 km off Honnavar and at 6, 25 and 105 km off Ratnagiri. The study area is exposed to open ocean waves from northwest to south, and the nearest landmass is ~ 1500 km in the northwest, ~ 2000 km in the west, ~ 4000 km southwest and ~ 9000 km in the south (Amrutha et al., 2016a). Due to its exposure to the Southern Oceans and the large fetch available, swells are present all year round in the study area and the swells are dominant during the non-monsoon period (Glejin et al., 2013). During February to May, due to the low wind-seas, the swells propagating from the southern hemisphere reach the eastern AS (Semedo et al., 2011; Glejin et al., 2013). Amrutha et al. (2016a) studied the changes in nearshore waves during the active sea/land breeze period (February-April) of the study area and reported that due to the influence of the land/sea breeze system, the range of the peak wave period in one day varied up to 8 s.

2.2 Data and methodology

The wave data from directional waverider buoys moored at 15 m water depth (15.842° N; 73.563° E) and at 5 m water depth (15.844° N; 73.625° E) off Vengurla in 2014 and 2015 are used in the study (Fig. 1). The buoys are at a distance of 6.64 km apart, and the buoy at 5 m water depth is 0.44 km from the coastline (Amrutha et al., 2016a). The wave data collected in October at other locations (Ratnagiri, Karwar and Honnavar) off the central west coast of India (Fig. 1) during 2010 to 2015 are also used in the study. The position and the water depth at the measurement locations are presented in Table 1. The heave and the eastward and northward displacement data recorded continuously at 1.28 Hz by the Datawell waverider buoy from 1 to 31 October in different years are used for the

study. The details of the data analysis are presented in Amrutha et al. (2015). Data covering 30 min are processed as one record. Zero-crossing analysis of the surface elevation time series is done to estimate the individual wave heights and periods. The H_{m0} , the peak wave period (T_p) and the mean wave period (T_{m02}) are derived from the wave spectrum. Following Kuik et al. (1988), the mean wave direction (D_m) at the spectral peak frequency (f_p) is estimated. The nautical convention is followed to represent directions. Maximum Entropy Method (MEM) is used to estimate the wave directional spectra (Lygre and Krogstad, 1986). The wave spectra are partitioned at periods 4 s and 15 s and the spectral energy for period more than 15 s are considered as due to long-period swells. ERA-Interim, the reanalysis product of ECMWF (European Centre for Medium-Range Weather Forecasts) (Dee et al., 2011) is used for examining the wave conditions in the Indian Ocean.

Third-generation spectral wave model WAVEWATCH III (WW3) version 4.18 (Tolman, 1991; 2009) is used to generate the spatial plot of peak wave period. WW3 multi model run with a resolution of $0.1^\circ \times 0.1^\circ$ in latitude and longitude covering the Northern Indian Ocean ($65^\circ \text{ E} - 90^\circ \text{ E}$ and $5^\circ \text{ N} - 25^\circ \text{ N}$) which is nested in the $0.5^\circ \times 0.5^\circ$ Indian Ocean domain ($20^\circ \text{ E} - 112^\circ \text{ E}$ and $70^\circ \text{ S} - 35^\circ \text{ N}$) is forced with surface wind fields from ERA-Interim at every 6 h interval with a spatial resolution of 0.5° . Wave frequencies were discretized over 25 bins on a logarithmic scale from 0.04 to 0.5 Hz; wave direction was binned into 36 intervals of 10° each. Seemanth et al. (2016) reported over North Indian Ocean during non-monsoon seasons, when the region is dominated by swells propagating from the south, Kahma and Calkoen (1992) stable parameterization scheme of Tolman and Chalikov (1996) is the better option for input and dissipation source function for estimation of H_{m0} . Amrutha et al. (2016b) observed that for estimation of wave period, ST4 (source term) physics (Ardhuin et al., 2010) gave good level of accuracy and hence the same is used in the study. The measured wave data at 3000 m water depth at a location (15.0000° N ; 69.0000° E) in the central AS is used to compare the model results in deep waters (Fig. 3). For comparison of the model results at 15 m water depth, the wave data collected at Karwar is used. Three error measurements; Root Mean Square Error (RMSE), BIAS and Pearson's correlation coefficient (r) are used to evaluate the performance of the model. At both the deep and shallow locations, the H_{m0} shows good comparison with RMSE of 0.13 to 0.2 m and BIAS of 0.01 to 0.13 m, and the estimated peak wave period is with RMSE of 2.3 to 2.7 s and BIAS of -0.4 to 0.4 s (Fig. 3).

3. Results and discussion

The wave condition in the study area during October is low to moderate with maximum values around 2 m. In 2013, the summer monsoon influence was present up to 10 October and hence the monthly average H_{m0} was higher (~ 0.76 m) compared to that in 2014 (~ 0.63 m) and in 2015 (~ 0.67

m). H_{m0} up to 2.1 m was measured in the first week of October 2013 (Fig. 4a). Due to the tropical cyclone (TC) Nilofar, high waves ($H_{m0} > 1$ m) are observed during 25-28 October 2014 (Figs. 4b and 4d); otherwise, the average H_{m0} during 1-20 October 2014 is 0.55 m. TC Nilofar originated from a low-pressure area in the AS that intensified into a tropical depression. The TC was formed on 25 October 2014 and moved northward as it grew stronger (Kazeminezhad, 2015). In 2015, during 7-12 October, relatively high waves ($H_{m0} > 1$ m) are observed due to the deep depression formed in the AS (IMD, 2015). Mean wave periods range from 3 to 10 s, with the mean value around 6 s. Once the summer monsoon/TC influence is reduced, long-period waves ($T_p > 18$ s) are observed at regular intervals (Fig. 4). During the TC period in 2014, when the H_{m0} is high (> 1 m), the long-period waves are almost absent (Fig. 4). The occurrence of these long-period waves is 7 times each in 2013 and 2015 and 5 times in 2014. At Vengurla during October, H_{m0} of the long-period swells are less than 1 m and the waves with $H_{m0} > 1$ m has $T_p < 12$ s (Fig. 4).

We have examined the wave data collected in October at other coastal locations (Ratnagiri, Karwar, and Honnavar) off the central west coast of India (Fig. 1) during 2010 to 2015 and observed the presence of the long-period waves at these locations also (Fig. 5). Ratnagiri is 130 km north of Vengurla, Karwar is 130 km south of Vengurla and Honnavar is 220 km south of Vengurla. The H_{m0} up to 1.4 m are observed for the long-period swells during 2010 to 2015 at Ratnagiri, Karwar, and Honnavar (Fig. 5). The spatial distribution of peak wave period in the Indian Ocean based on wave model WW3 from 7 to 12 October 2014 is presented in Figure 6. A storm in the area bounded by 40-60° S and 20-40° E during 4-6 October 2014 (Fig. 7) generated the high waves and these waves propagated and reached the study area on 11 October 2014 (Fig. 6). The study shows that the presence of long-period swells along the 350 km stretch of the eastern AS is almost in the same day (Figs. 6 & 8). Off the southwest coast of India, there is a region where the long-period waves are not present due to the presence of Maldives Islands, but close to the coast, long-period waves are present (Fig. 6). Alves (2006) observed that global wave climate is influenced by the waves generated along the Southern Ocean storm belt due to the swell propagation. The examination of ERA-Interim waves at different locations in the AS and Indian Ocean reveals that high waves ($H_{m0} > 4$ m) generated in the south Indian Ocean (40-60° S; 20-40° E) reached the measurement locations in 5 to 6 days and resulted in the long-period swells (Fig. 6). For wave frequency (f) = 0.067 Hz, the energy advection speed (C_g) = $0.5g/2\pi f = 11.7$ m/s and it will take such waves 6-7 days to traverse the distance of ~7000 km. Amrutha et al. (2015) observed that during the pre-monsoon period also long-period swells ($T_p \sim 18$ s) arrived in distinct trains lasting about 5 days in the central west coast of India. Kumar et al. (2012) also observed the arrival of swells ($T_p > 10$ s) in distinct trains lasting about 5

days during pre-monsoon (May 2009). The measured wave data at 3000 m water depth at a location (15.0000° N; 69.0000° E) in the central AS shows that T_p has similar values in the deep water (~3000 m water depth) and at 9 m water depth. Fig. 9 shows that the long-period waves are also observed in the deep water. From 3000 m to 9 m water depth, a significant reduction is observed in H_{m0} (Fig. 9).

The normalisation of each spectrum is carried out by dividing the wave spectral energy density by the corresponding maximum spectral energy density and the contour plots of normalised wave spectral energy density in frequency-time domain are presented to understand the spread of spectral energy in different frequency (Fig. 10). During the high waves ($H_{m0} > 1$ m), most of the wave energy is concentrated between 0.1 and 0.2 Hz for low waves ($H_{m0} < 1$ m) the spectral wave energy is in lower frequencies (< 0.1 Hz). The present study shows that with the interaction of wind-sea with long-period swells, the frequency of the peak wave energy gradually shifted towards high-frequency region (Fig. 10). The spectrum during the occurrence of the long-period wave is narrow banded. As the local wind increased, as expected the peak wave period shifted towards lower values. The pattern is similar at 15 and 5 m water depth. Similar shifting of peak frequency is observed at Ratnagiri, Karwar and Honnavar in different years (Fig. 11). The long-period waves have direction $< 240^\circ$, whereas the high-frequency waves have direction $> 240^\circ$ (Fig. 10).

At the study region, the contributions of infragravity waves ($T > 25$ s) are small ($< 0.4\%$) relative to the wind-sea and swell (Table 2). From the spectrum, it can be noted that most of the energy (~67 to 78%) is between 0.065 and 0.25 Hz (Table 2). About 6 to 9% of the wave spectra are with T_p more than 18 s and 34-38% are with T_p more than 15 s. High values of inverse wave age (ratio of sea surface wind speed to speed of the wave corresponding to peak frequency) indicate regions where the waves are strongly coupled to the local wind field and low values indicate regions where swells are present (Hanley et al. 2010). In October, the inverse wave age varies from 0.2 to 0.5 indicating that the sea state of study region become mixed state ($0.15 < \text{inverse wave age} < 0.83$; both wind driven wave and wave driven wind are present) (Hanley et al., 2010). In shallow water (5m water depth), the inverse wave age values are higher (~0.4) than that observed at 15 m water depth (~0.3). 11 to 22% of the total spectral energy is available above 0.25 Hz. Relatively high percentage of waves in frequency higher than 0.25 Hz is observed in 2012 compared to other years. Relatively low percentage of short-period waves are observed in 2015 and 2011 compared to other years (Table 2).

Earlier studies show that wave heights of different regions of ocean are linked with climate indices; i) Southern Annular Mode (Hemer et al., 2010), ii) ENSO (Gulev and Grigorieva 2004) and iii) IOD

(Anoop et al., 2016). Since ENSO and IOD events manifest most strongly during late boreal fall and early winter (October-November), they influence the post-monsoon waves. The years 2011 and 2015 are positive IOD years and during the positive IOD year a decrease in northwest wind is expected (Anoop et al., 2016). But the significant wave height anomaly in October did not show a negative value in 2011 and 2015 since the waves in the study area consists of swells apart from the wind-sea (Fig. 12).

To study the wave spectral characteristics at 5 and 15 m water depth, monthly averaged wave spectrum is estimated from the half-hourly data during 1-20 October 2014, by taking the mean of the spectral energy density at the corresponding frequencies. Averaged wave spectrum at 5 and 15 m water depth during 1-20 October 2014 shows double peaks with the primary peak corresponding to the swells (~ 0.07 Hz) from 225° and the secondary peak of wind-sea (~ 0.2 Hz) from west (Fig. 13a & 14). During the pre-monsoon period (FMAM), both at 15 and 5 m water depth, the predominant peak is at 0.074 Hz and the secondary peak was at 0.174 (at 5 m water depth) and 0.187 Hz (at 15 m water depth) (Amrutha et al. 2016a). The spectral energy density is higher at 15 m water depth than at 5 m and the difference is large in the wind-sea region (Fig. 13a). Also, the difference in the spectral energy density between 15 and 5 m water depth is less at swell peak than that observed at the wind-sea peak. Due to the TC Nilofar, the secondary wind-sea peak is not predominant in monthly average spectrum (1-31 October), instead another predominant peak is formed in the swell region at 0.1 Hz. The 99 and 90 percentile wave spectra are computed to know the spectral shape of the spectra representing 99% and 90% of all the spectra during a month. The 99 and 90 percentile wave spectra are also double-peaked and show the predominant peak at ~ 0.07 Hz, a secondary peak at ~ 0.2 to 0.25 Hz (Fig. 13b). Even though both the wind-sea and swell dominated spectra are observed in the inter-monsoon period, the mean wave spectrum during the study period shows swell dominated spectra and the energy at wind-sea peak is minimum during 2015 (Fig. 14).

In October, the multi-peak spectra during the long-period swell dominated period represent independent wave systems corresponding to long-period swells generated by remote storms, swells generated by nearby storms and locally generated wind waves. Hence, the mean wave direction varied from 194 to 288° . The wind-sea from 240 to 300° due to local winds are superimposed on the low-amplitude swells from 210 to 240° (Fig. 10) and is similar in both years except during the TC period. During the TC period, the wind-seas were from 240 to 270° . At 5 m water depth, the wind-sea is mainly from 240 to 270° . A similar observation was made during the pre-monsoon period (February and March) by Amrutha et al. (2016a).

During February-April, diurnal variation in wave parameters due to the sea breeze are reported off the central west coast of India (Neetu et al., 2006; Vethamony et al., 2011; Glejin et al., 2013). The present study shows that the diurnal variations in H_{m0} in October is less than 0.1 m, but the variations in T_{m02} is up to 2.5 s (Fig. 15) and is similar to the observation of Kumar and Anjali (2015) off Honnavar. At 15 m water depth, the maximum H_{m0} is observed between 13 and 14 UTC and the minimum T_{m02} and maximum short-period wave is observed during 12 and 13 UTC (Fig. 15). There is significant diurnal variation ($\sim 10\%$) in the short period waves due to the sea breeze. At 5 m water depth, the maximum H_{m0} , minimum T_{m02} and maximum short-period waves are observed between 11 and 12 UTC. The study shows that the amplification in wave height due to sea breeze is slightly earlier at 5 m water depth compared to 15 m.

Apart from the land/sea breeze influence, significant diurnal variations in wave parameters are also observed in October. The range of H_{m0} in a day varied up to 0.7 m during the tropical cyclone and up to 0.3 m in other periods (Fig. 16), whereas the variation in T_{m02} is less (< 4 s) during the tropical cyclone compared to other periods (~ 6 s). For mean wave direction, variation up to 30° is observed at 5 m water depth, but at 15 m water depth at few occasions large variation ($\sim 130^\circ$) is observed due to the change in the swell/wind-sea predominance.

In 2013, contribution of short period waves (wave period, $T < 6$ s, dominated by local seas) in the measured waves is 36% and reduced to 25% in 2015 (Fig. 15). Accordingly the contribution of long period waves ($T > 12$ s, primarily swells) increased from 22% in 2013 to 30% in 2015 and the intermediate period waves ($6 \text{ s} \leq T \leq 12 \text{ s}$, mixture of local and regional wind forcing) increased from 42% in 2013 to 46% in 2015. The wave period associated with a wave height is required while planning the marine facility. The joint distribution of wave period and height is presented in Figure 17. The high waves ($H_{m0} > 1$ m) are associated with peak wave period 6-12 s and waves with low height ($H_{m0} < 1$ m) are associated with wide range of peak wave period (5-22 s) due to the fact that the measurements were carried out in open ocean and swells that have originated from a distant storm might have decayed with time resulting in low wave height whereas the wave period remains high (Kumar et al., 2010).

4. Conclusions

In the present study, we have illustrated the presence of long-period swells in the eastern AS during the fall inter-monsoon period based on measured wave data from moored directional wave rider buoys at different locations during 2010-2015. In the inter-monsoon period, the sea state of the eastern Arabian Sea is generally low to moderate (significant wave height < 1 m). But high waves

are also observed during the inter-monsoon period due to the tropical cyclone or due to the extension of summer monsoon to the first week of October. In October, the sea state of study region becomes mixed state, i.e. both wind driven wave and wave driven wind are present. About 34 to 38% of the wave spectra are with peak wave period more than 15 s. Relatively high percentage of long-period waves are observed in 2015 and 2011 (positive Indian Ocean Dipole years) compared to other years due to the decrease in the northwest short period waves. The diurnal variations in significant wave height in October are less than 0.1 m, whereas the changes in mean wave period are up to 2.5 s. In the study area, during the inter-monsoon period, the wind-seas from 240 to 300° due to local winds are superimposed on the long-period swells from southwest (210 to 240°). The role of equatorial Indian Ocean dynamics on the long-period swells, which is very active during October and has strong interannual variability is not examined in the present study and the mechanism for the interannual variability in both long period waves and short period waves need more detailed study.

Acknowledgments

The authors acknowledge the Earth System Science Organization, Ministry of Earth Sciences, New Delhi for providing the financial support to conduct part of this research. The facilities to carry out the study were made available by the Director, CSIR-NIO. We thank Dr. R. S. Kankara, Head, Coastal Processes & Shoreline Management, ICMAM-PD, Chennai, Dr. T.M. Balakrishnan Nair, Head OSISG, Mr. Arun Nherakkol, Scientist, INCOIS, Hyderabad and Mr. Jai Singh, Technical Assistant, CSIR-NIO for the help during data collection. We thank Dr. Bhat and Dr. J. L. Rathod, Department of Marine Biology, Karnataka University PG Centre, Karwar and Dr. Vedpathak and Mr. Parag Kulkarni, Centre for Coastal & Marine Biodiversity, Dr. Babasaheb Ambedkar Marathwada University, Ratnagiri for providing the logistics required for wave data collection at Karwar and Ratnagiri. This research would not have been complete without the availability of the ERA-Interim data provided by the ECMWF. The authors would like to thank both the reviewers and the editor for the suggestions for improvement of this article. This publication is NIO contribution xxxx.

References

- Alves, J.H.G., 2006. Numerical modeling of ocean swell contributions to the global wind-wave climate. *Ocean Modell.*, 11(1), 98–122.
- Amrutha, M.M., Kumar, V.S., Sharma, S., Singh, J., Gowthaman, R., Kankara, R.S., 2015. Characteristics of shallow water waves off the central west coast of India before, during and after the onset of the Indian summer monsoon. *Ocean Engineering*, 107, 259-270. doi:10.1016/j.oceaneng.2015.07.061.

Amrutha, M.M., Kumar, V.S., Singh, J., 2016a. Changes in nearshore waves during the active sea/land breeze period off Vengurla, central west coast of India. *Annales Geophysicae*, 34,1-12, doi:10.5194/angeo-34-1-2016.

Amrutha, M.M., Kumar, V.S., Sandhya, K.G., Balakrishnan Nair, T.M., Rathod, J.L. 2016b. Wave hindcast studies using SWAN nested in WAVEWATCH III - comparison with measured nearshore buoy data off Karwar, eastern Arabian Sea, *Ocean Engineering* 119C, 114-124.

Anoop, T.R., Kumar, V.S., Shanas, P.R., Glejin Johnson, Amrutha, M.M., 2016. Indian Ocean Dipole modulated wave climate of eastern Arabian Sea. *Ocean Science*, 12, 369-378, doi:10.5194/osd-12-2473-2015.

Anoop, T.R., Kumar, V.S., Shanas, P.R., Johnson, G., 2015. Surface wave climatology and its variability in the North Indian Ocean based on ERA-Interim reanalysis. *Journal of Atmospheric and Oceanic Technology*, 32, 1372-1385. doi: 10.1175/JTECH-D-14-00212.1.

Ardhuin, F., Chapron, B., Collard, F., 2009. Observation of swell observed across oceans. *Geophys. Res. Lett.*, 36, 1-5.

Ardhuin, F., Rogers, E., Babanin, A.V., Filipot, J.-F., Magne, R., Roland, A., van der Westhuysen, A., Queffelec, P., Lefevre, J.-M., Aouf, L., Collard, F., 2010. Semi-empirical Dissipation Source Functions for Ocean Waves. Part I: Definition, Calibration, and Validation. *J. Phys. Oceanogr.*, 40, 1917–1941.

Dee, D. P., Uppala, S. M., Simmons, A. J., Berrisford, P., Poli, P., Kobayashi, et al., 2011. The ERA-Interim reanalysis: Configuration and performance of the data assimilation system. *Q. J. R. Meteorol. Soc.*, 137(656), 553-597.

Dora, G.U., Kumar, V.S., 2015. Sea state observation in island-sheltered nearshore zone based on in situ intermediate-water wave measurements and NCEP/CFSR wind data. *Ocean Dynamics*, 65(5), 647-663, doi: 10.1007/s10236-015-0822-1.

Gjevik, B., Rygg, O., Krogstad, H.E., Lygre, A., 1988. Long period swell wave events on the Norwegian Shelf. *Journal of Physical Oceanography*, 18(5), 724–737.

Glejin, J., Kumar, V.S., Amrutha, M.M., Singh, J., 2016. Characteristics of long-period swells measured in the in the near shore regions of eastern Arabian Sea. *International J of Naval Architecture and Ocean Engineering*, 8, 312-319.

Glejin, J., Kumar, V.S., Chempalayil, S.P., Singh, J., Pednekar, P., Kumar, K.A., Dora, G.U., Gowthaman, 2012. Variations in swells along eastern Arabian Sea during the summer monsoon. *Open Journal of Marine Science*, 2, 43-50.

Glejin, J., Kumar, V.S., Nair, T.M.B., and Singh, J., 2013. Influence of winds on temporally varying short and long period gravity waves in the near shore regions of the eastern Arabian Sea. *Oce. Sci.*, 9, 343–353.

Gulev, S.K., Grigorjeva, V., 2004. Last century changes in ocean wind wave height from global visual wave data. *Geophys. Res. Lett.*, 1:31(24).

Hanley, E.K., Stephen, E.B., Peter, P.S., 2010. A global climatology of wind-wave interaction. *J Phys Oceanogr*, 40(6),1263–1282.

- Hastenrath, S., Nicklis, A., Greischar, L., 1993. Atmospheric-Hydrospheric Mechanisms of Climate Anomalies in the Western Equatorial Indian Ocean. *Journal of Geophysical Research*, 98(C11), 20219-20235.
- Hemer, M.A., Church, J.A., Hunter, J.R., 2010. Variability and trends in the directional wave climate of the Southern Hemisphere. *International Journal of Climatology*, 30(4), 475-91.
- Kahma, K. K., & Calkoen, C. J., 1992. Reconciling discrepancies in the observed growth of wind-generated waves. *Journal of Physical Oceanography*, 22(12), 1389-1405.
- Kazeminezhad, M.H., Ghavanini, F.A., 2015. Numerical modelling of cyclone-induced waves using WAVEWATCH IIITM. E-proceedings of the 36th IAHR World Congress 28 June – 3 July, 2015, The Hague, the Netherlands, 1-7.
- Kuik, A.J, Van Vledder, G.P., Holthuijsen, L.H., 1988. A method for the routine analysis of pitch-and-roll buoy wave data. *Journal of Physical Oceanography*, 18(7), 1020-1034.
- Kumar, V.S., Anand, N.M., Kumar K.A., Mandal, S., 2003. Multi peakedness and groupiness of shallow water waves along Indian coast. *J. Coastal. Res.*, 19, 1052-1065.
- Kumar, V.S., Anjali N., 2015. Inter-annual variations in wave spectral characteristics at a location off the central west coast of India. *Annales Geophysicae*, 33, 159-167, www.ann-geophys.net/33/159/2015/
- Kumar, V.S., Johnson, G., Dora, G.U., Chempalayil, S.P., Singh, J., Pednekar, P., 2012. Variations in nearshore waves along Karnataka, west coast of India. *J. Earth. Syst. Sci.*, 121, 393-403. doi:10.1007/s12040-012-0160-3.
- Kumar, V.S., Kumar, K.A., Anand, N.M., 2000. Characteristics of waves off Goa, west coast of India. *Journal of coastal research*, 782-789.
- Kumar, V.S., Philip, S.C., Nair, T.N.B., 2010. Waves in shallow water off west coast of India during the onset of summer monsoon. *Annales Geophysicae*, 28, 817–824. doi:10.5194/angeo-28-817-2010.
- Kumar, V.S., Shanas, P.R., Dubhashi, K.K., 2014. Shallow water wave spectral characteristics along the eastern Arabian Sea. *Natural Hazards*, 70(1), 377–394, doi 10.1007/s11069-013-0815-7.
- Kumar, V.S., Singh, J., Pednekar, P., Gowthaman, R., 2011. Waves in the nearshore waters of northern Arabian Sea during the summer monsoon. *Ocean Engineering*, 38(2), 382-388.
- Lygre A., Krogstad H.E., 1986. Maximum Entropy Estimation of the Directional Distribution in Ocean Wave Spectra, *Journal of Physical Oceanography*, 16, 2052-2060.
- Madden, R. A., Julian, P. R., 1971. Detection of a 40-50 day oscillation in the zonal wind in the tropical Pacific. *Journal of the Atmospheric Sciences*, 28(5), 702-708.
- McComb, P., Johnson, D.L., and Beamsley, B., 2009. Numerical study of options to reduce swell and long wave penetration at Port Geraldton. *Proceedings of the 2009 Pacific Coasts and Ports Conference*, Wellington, New Zealand.
- Mehta, A. V., & Krishnamurti, T. N., 1988. Interannual variability of the 30 to 50 day wave motions. *Journal of the Meteorological Society of Japan*, 66(4), 535-548.

Munk, W. H., Miller, G. R., Snodgrass, F. E., and Barber, N. F., 1963. Directional recording of swell from distant storms. *Philosophical Transactions of the Royal Society of London*, 255(1062), 505-584.

Neethu, S., Shetye Satish, Chandramohan, P., 2006. Impact of sea breeze on wind-seas off Goa, west coast of India. *Journal of Earth System Science*, 115, 229-234.

Pattanaik, D.R., Mohapatra, M., Mukhopadhyay, B., Tyagi, A., 2013. A preliminary study about the prospects of extended range forecast of tropical cyclogenesis over the north Indian Ocean during 2010 post-monsoon season. *Mausam*, 64(1), 171-188.

Rao, S. A., Behera, S. K., Masumoto, Y., & Yamagata, T., 2002. Interannual subsurface variability in the tropical Indian Ocean with a special emphasis on the Indian Ocean dipole. *Deep Sea Research Part II: Topical Studies in Oceanography*, 49(7), 1549-1572.

Saji, N. H., Goswami, B. N., Vinayachandran, P. N., Yamagata, T., 1999. A dipole mode in the tropical Indian Ocean. *Nature*, 401(6751), 360-363.

Schott, F.A., McCreary, J.P., 2001. The monsoon circulation of the Indian Ocean. *Progress in Oceanography* 51.1: 1-123.

Schott, F.A., Xie, S.P., McCreary, J.P., 2009. Indian Ocean circulation and climate variability. *Reviews of Geophysics*, 1:47(1). doi:10.1029/2007RG000245.

Seemanth, M., Bhowmick, S.A., Kumar, R., Sharma, R., 2016. Sensitivity analysis of dissipation parameterizations in a third-generation spectral wave model, WAVEWATCH III for Indian Ocean. *Ocean Eng.* 124, 252-273.

Semedo, A., Sušelj, K., Rutgersson, A., Sterl, A., 2011. A global view on the wind sea and swell climate and variability from ERA-40. *J. Clim.*, 24 (5), 1461-1479.

Shetye, S.R., Shenoi, S. S. C., Antony, M. K., Kumar, V. K., 1985. Monthly-mean wind stress along the coast of the north Indian Ocean. *J. Earth Syst. Sci.*, 94, 129-137, doi:10.1007/BF02871945.

Tolman, H. L., 1991. A third-generation model for wind waves on slowly varying, unsteady and inhomogeneous depths and currents. *J. Phys.Oceanogr.*, 21, 782-797.

Tolman, H. L., 2009. User manual and system documentation of WAVEWATCH III TM version 3.14. Tech. Note., 276, NOAA/NWS/NCEP/MMAB, 194p.

Tolman, H. L., Chalikov, D., 1996. Source terms in a third-generation wind wave model. *J. Phys.Oceanogr.*, 26, 2497-2518.

Vethamony, P., Aboobacker, V.M., Menon, H.B., Ashok Kumar, K., Cavaleri, L., 2011. Superimposition of wind seas on pre-existing swells off Goa coast. *J. Mar. Syst.*, 87, 47-54.

List of Figures

Figure 1. Map showing the locations of wave measurement. The big circle represent the nearshore buoy and the small circle is the deep water buoy location

Figure 2. Left panel shows the wind climatology in Arabian Sea during January, April, July and October and the right panel shows the wave climatology during the same period. ERA-Interim reanalysis data during 1979 to 2015 is used

Figure 3. Comparison of simulated peak wave period and significant wave height with the measured data. Left panel is for deep water location and right panel is for shallow water location

Figure 4. Time series plot of significant wave height and wind speed (left panel) and peak wave period (right panel) at 15 m water depth in October during 2013 to 2015 (a to c) and at 5 m water depth during 2014 and 2015 (d to e) based on measured data

Figure 5. Time series plot of significant wave height and peak wave period from 2010 to 2015 based on measured data. Left panel shows the parameters at 13 m water depth off Ratnagiri, middle panel is for Karwar at 15 m water depth and the right panel is for that at 9 m water depth off Honnavar

Figure 6. Spatial distribution of spectral peak wave period in second based on numerical model WW3 in different time (5-12 October 2014)

Figure 7. Wind pattern in Indian Ocean from 4 to 6 October 2014. The arrows indicate the wind direction and the colour code indicates the wind speed in m/s

Figure 8. Left panel shows the concurrent occurrence of long-period waves at Ratnagiri, Honnavar and Karwar in October during 2010 to 2014 based on measured data. Right panel shows the significant wave height (H_{m0}) at Honnavar, at location 22.5° S, 62.5° E (based on ERA-Interim) and the box average H_{m0} for $40-60^\circ$ S, $20-40^\circ$ E along with the peak wave period (T_p) at Honnavar

Figure 9. Time series plot of a) significant wave height, b) peak wave period measured at 3000 and 9 m water depth and c) wind speed measured at 3000 m water depth and re-analysis NCEP/NCAR wind speed at 12.5° N; 72.5° E during October 2009

Figure 10. Top panel shows the temporal distribution of normalised spectral energy density with frequency in different years at 5 and 15 m water depth and bottom panel shows the distribution of wave direction with frequency based on measured data

Figure 11. Temporal distribution of normalised spectral energy density with frequency in different years. Top panel is for Ratnagiri, middle for Karwar and bottom panel is for Honnavar

Figure 12. Significant wave height anomaly in January, April, July and October during 2010 to 2015 in the Arabian Sea based on ERA-Interim data. The wave height contours are in m.

Figure 13. a) Mean and b) 99, 90 and 75 percentiles of one dimensional wave energy spectra for October 2014 at 15 and 5 m water depth

Figure 14. Monthly average directional spectra during 2013 to 2015. Left panel is for 15 m water depth and right panel is for 5 m water depth. The contours are spectral energy density (m^2/Hz) in log scale

Figure 15. Variation in $\frac{1}{2}$ hourly averaged wave parameters at 15 and 5 m water depth in different years; Left panel shows the significant wave height (H_{m0}) and mean wave period; right panel shows the percentage of long-period (LP) waves, percentage of intermediate period (IP) waves and percentage of short-period (SP) waves

Figure 16. Time series plot showing the range of wave parameters in a day; a) significant wave height (H_{m0}), b) mean wave period (T_{m02}), c) peak wave period (T_p) d) spectral width parameter and e) mean wave direction (D_m) at 15 and 5 m water depth during October 2014

Figure 17. Scatter plot of peak wave period with significant wave height at 15 and 5 m water depth off Vengurla in different years

Table 1. Measurement locations and the water depth

Location	Latitude	Longitude	Measurement duration	Water depth (m)
Ratnagiri	16.980° N;	73.258° E	1-31 October 2010 1-31 October 2011 1-31 October 2012 1-31 October 2013 1-31 October 2014 1-31 October 2015	13
Vengurla	15.842° N;	73.563° E	1-31 October 2013 1-31 October 2014 1-31 October 2015	15
Vengurla	15.844° N;	73.625° E	1-31 October 2014 1-31 October 2015	5
Karwar	14.821° N;	74.053° E	1-31 October 2010 1-31 October 2011 1-31 October 2012 1-31 October 2013 1-31 October 2014 1-20 October 2015	15
Honnavar	14.304° N;	74.391° E	1-31 October 2010 1-31 October 2011 1-31 October 2012 1-31 October 2013 1-31 October 2014 1-31 October 2015	9

Table 2. Percentage of wave spectral energy density in different period ranges and percentage of wave spectra with peak wave period more than 15 and 18 s in different years

Location	Year	Wave period range			Peak wave period			Number of data
		T > 25 s	25 > T > 15 s	15 > T > 4 s	T < 4 s	> 15 s	> 18 s	
Honnavar	2010	0.17	5.77	76.15	17.91	13.98	3.63	1488
	2011	0.38	18.86	69.20	11.55	32.86	9.14	1488
	2012	0.18	12.79	67.37	19.66	19.55	1.08	1478
	2013	0.23	13.67	68.27	17.83	31.85	7.33	1488
	2014	0.36	13.40	71.53	14.72	24.28	6.41	1483
	2015	0.28	18.98	66.24	14.50	38.37	9.48	1488
Karwar	2011	0.19	15.28	73.07	11.46	29.17	8.13	1488
	2012	0.12	13.32	71.85	14.71	21.57	0.40	1488
	2013	0.11	11.01	73.34	15.54	19.83	3.76	1488
	2014	0.16	11.15	76.04	12.65	17.85	4.65	1485
	2015	0.36	18.89	67.25	13.50	37.40	8.61	1344
Vengurla - 15 m	2013	0.10	8.10	74.95	16.85	16.26	1.68	1488
	2014	0.12	7.94	78.22	13.71	14.31	1.28	1488
	2015	0.16	14.73	73.33	11.78	33.53	5.17	1488
Vengurla-5 m	2014	0.30	10.81	74.43	14.45	18.08	3.36	1488
	2015	0.31	16.85	71.24	11.60	34.41	6.79	1488
Ratnagiri	2010	0.10	4.32	76.57	19.02	12.57	3.63	1488
	2011	0.26	13.14	69.63	16.96	30.78	8.60	1488
	2012	0.09	9.76	67.65	22.50	21.30	0.81	1488
	2013	0.10	9.35	74.36	16.19	25.47	4.64	1488
	2014	0.17	8.63	72.62	18.57	21.30	5.11	1488
	2015	0.16	16.14	68.81	14.88	35.15	6.85	1488

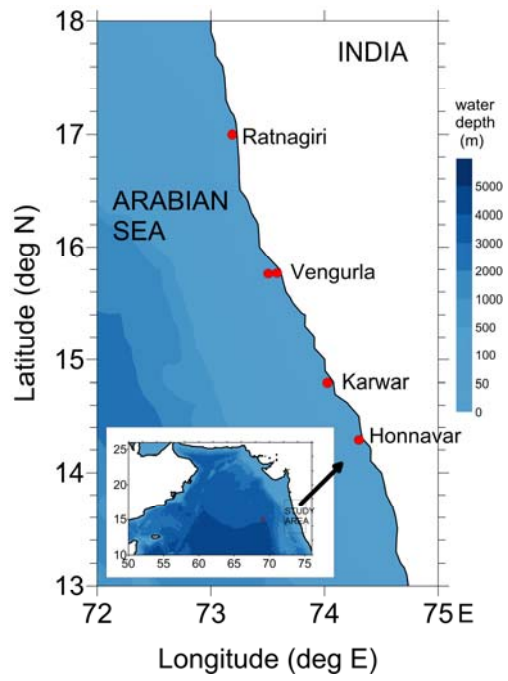


Figure 1.

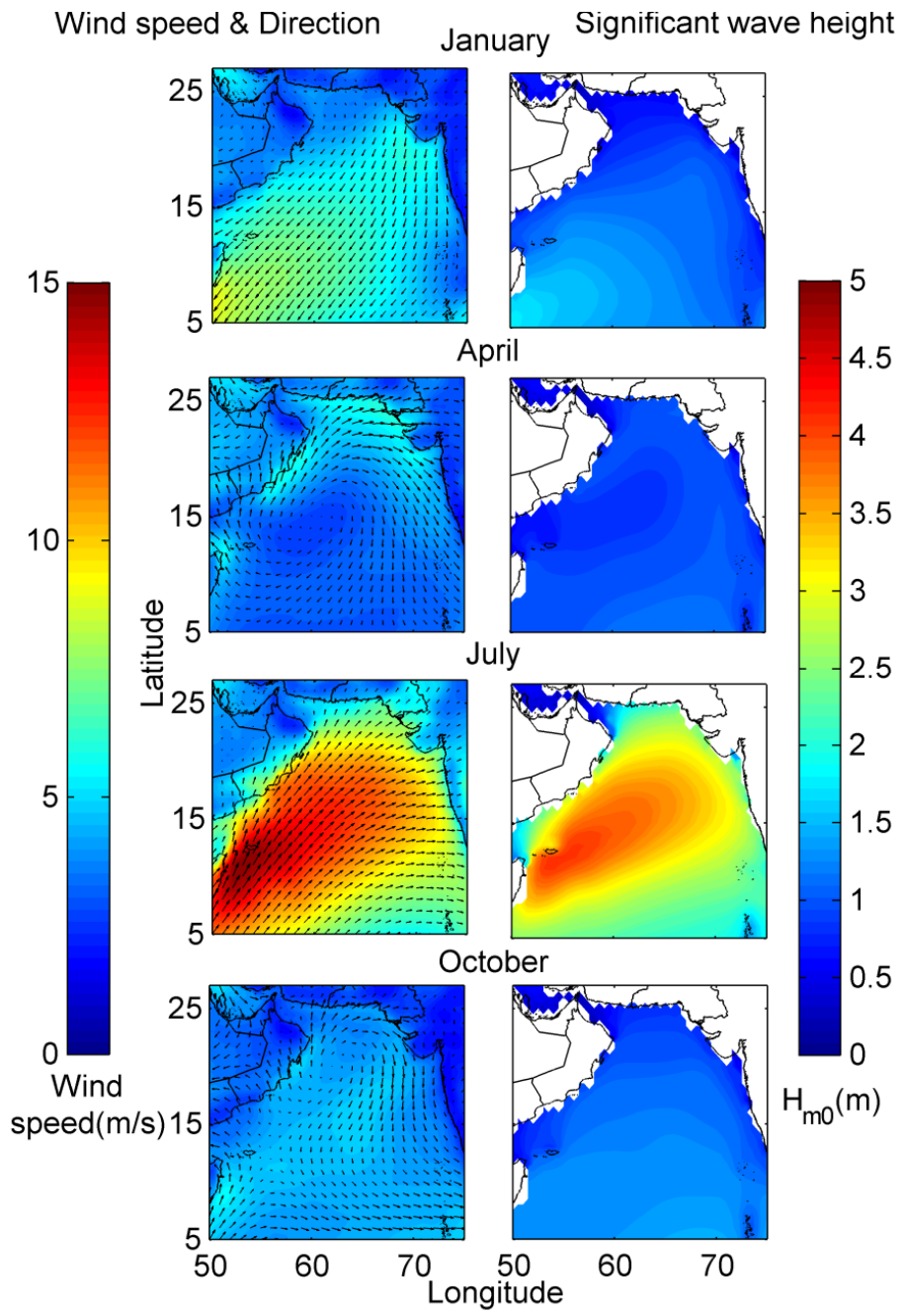


Figure 2.

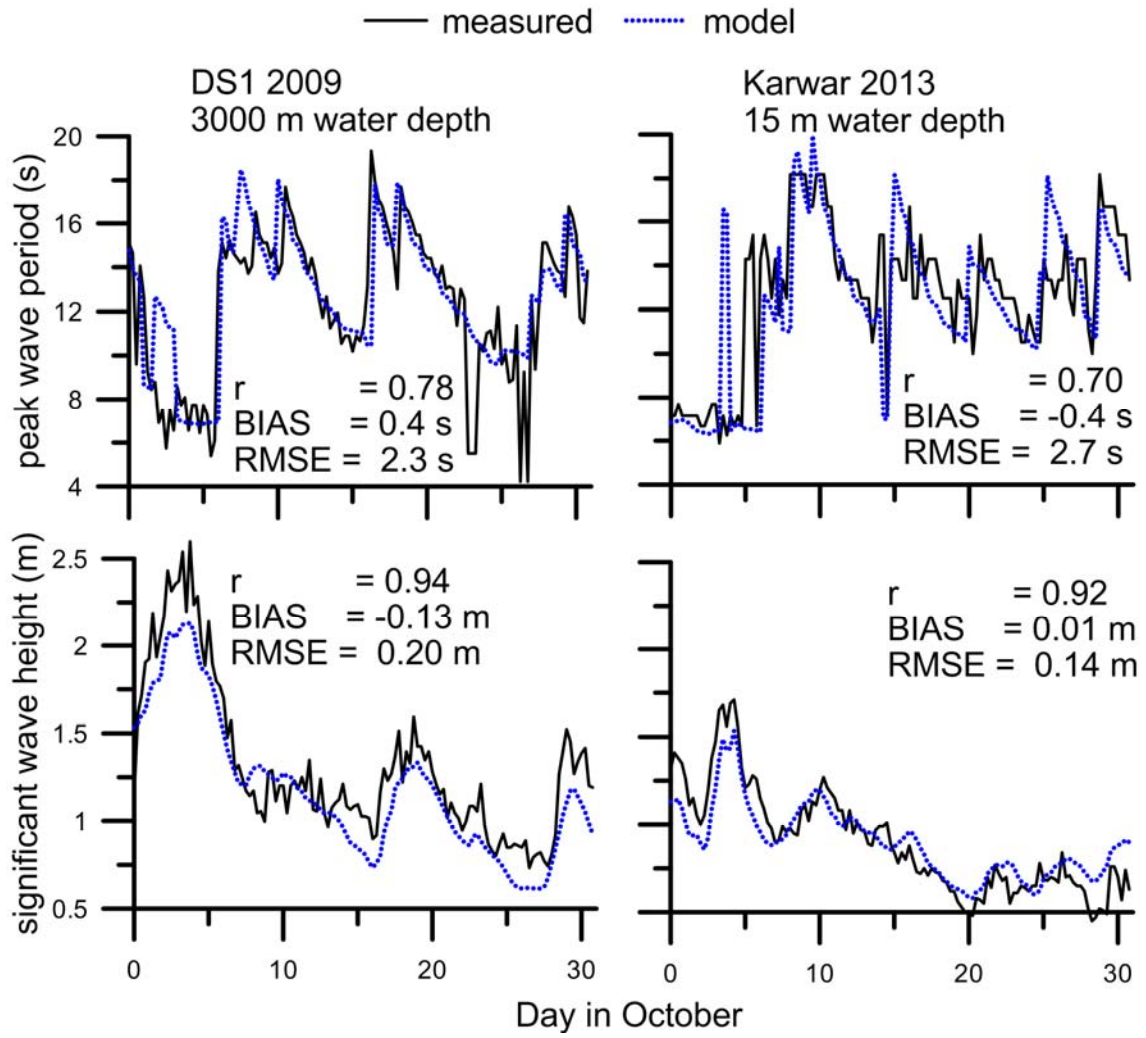


Figure 3

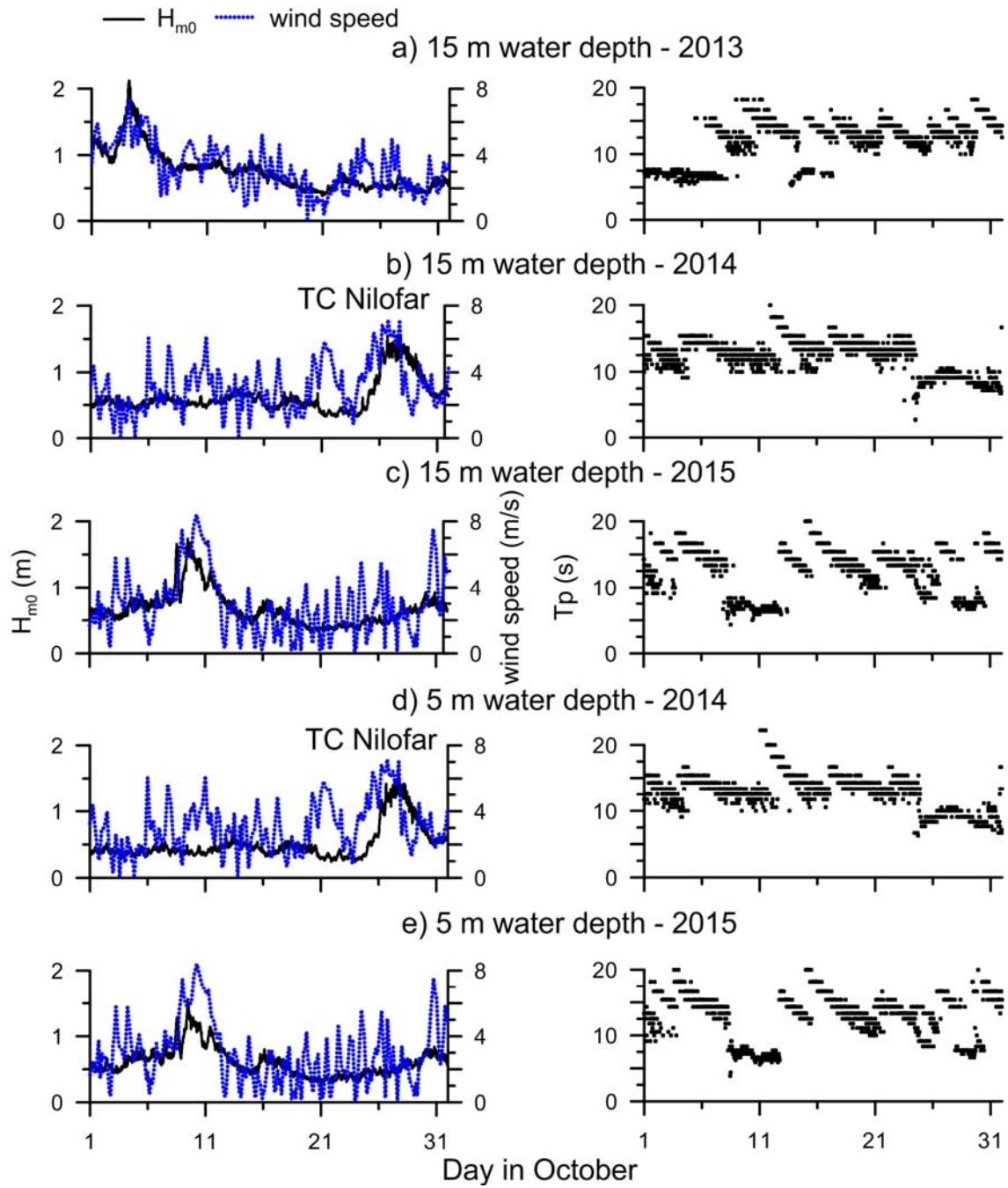


Figure 4.

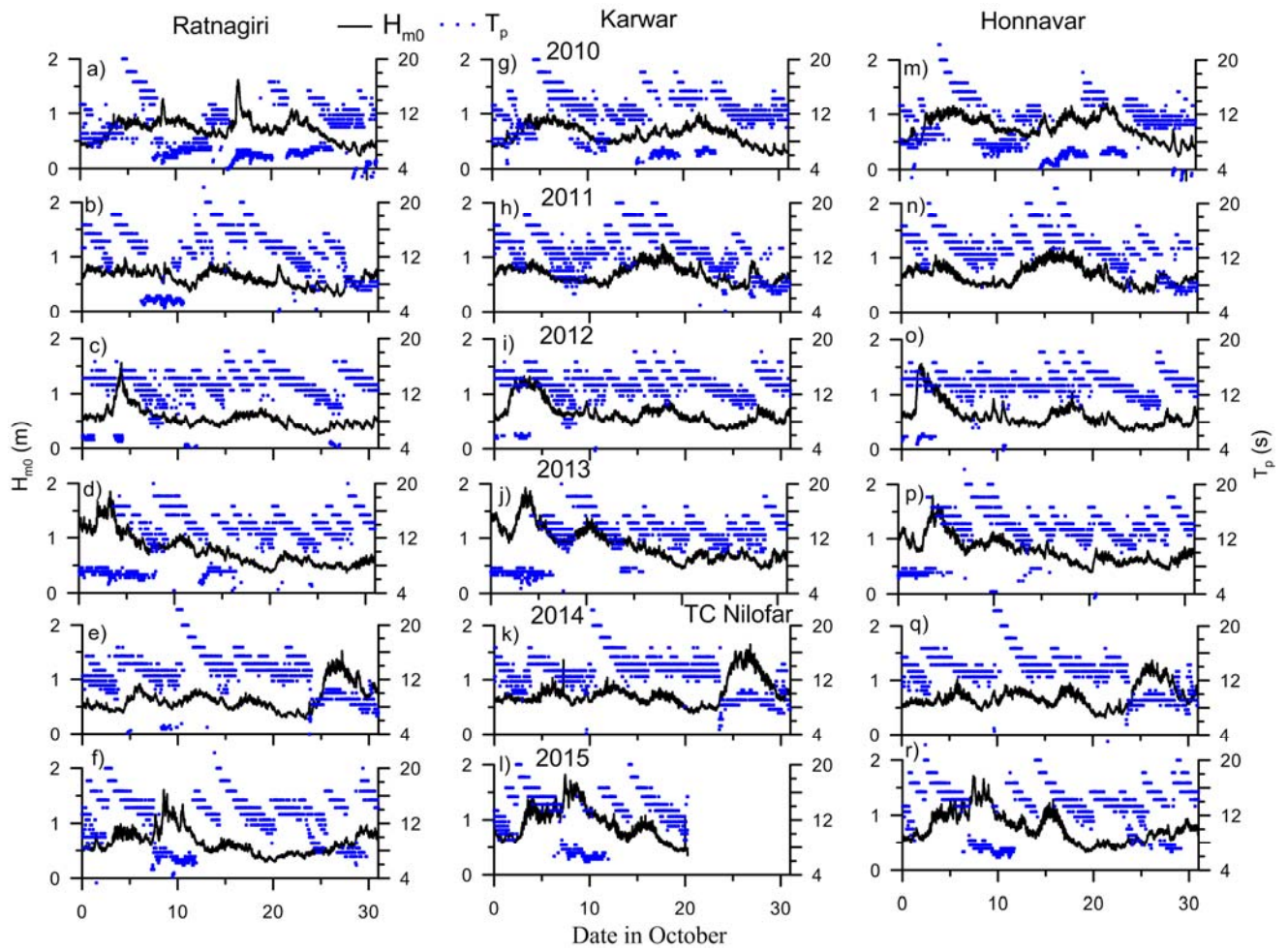


Figure 5.

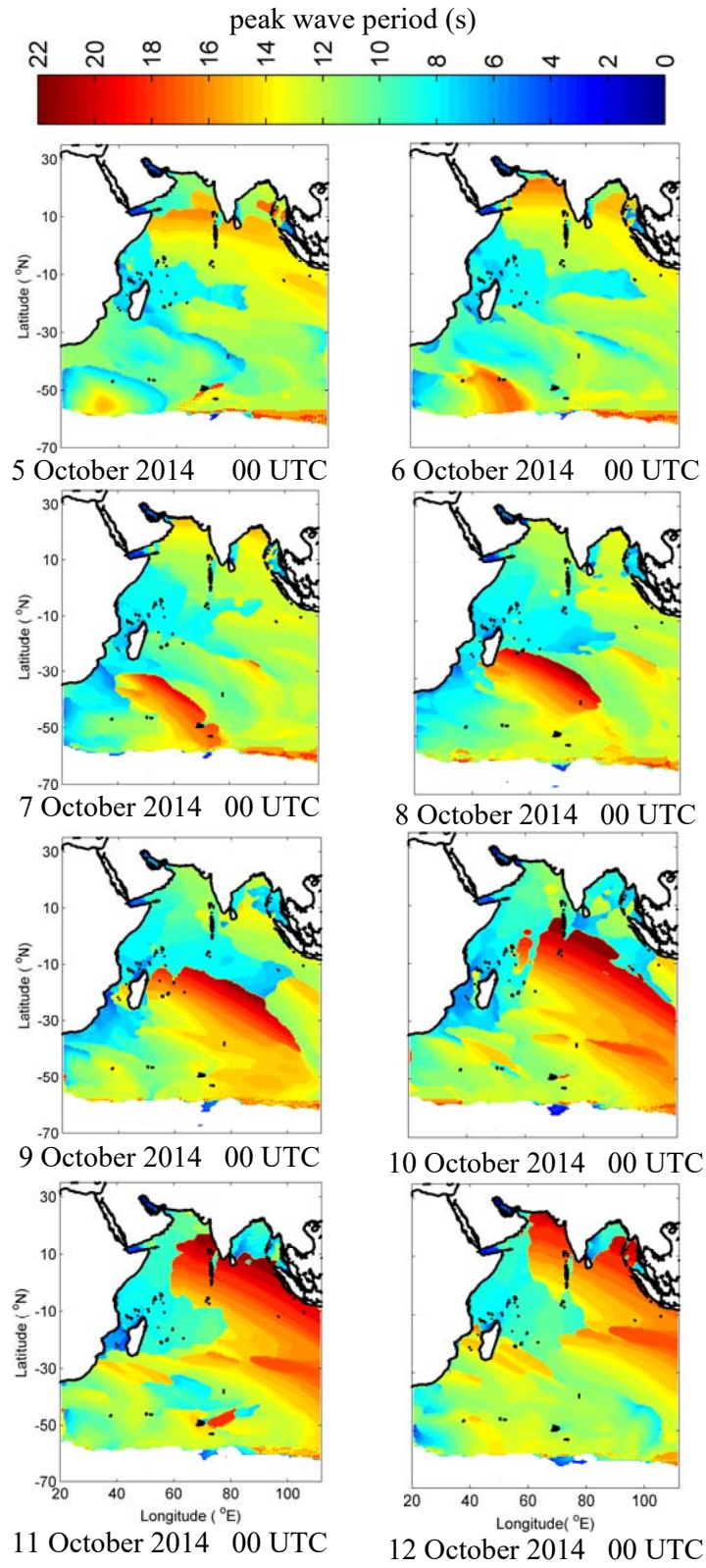


Figure 6.

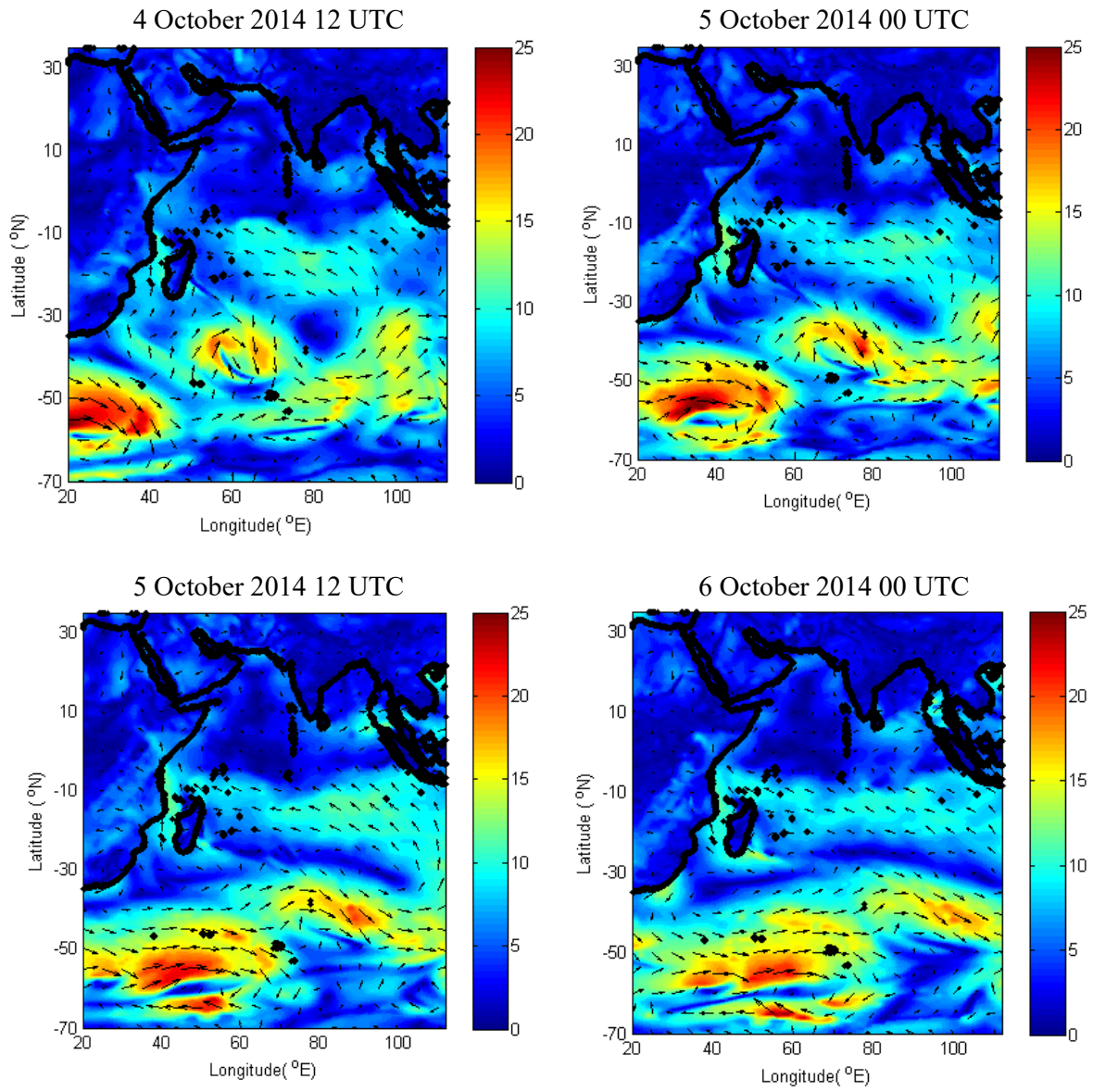


Figure 7.

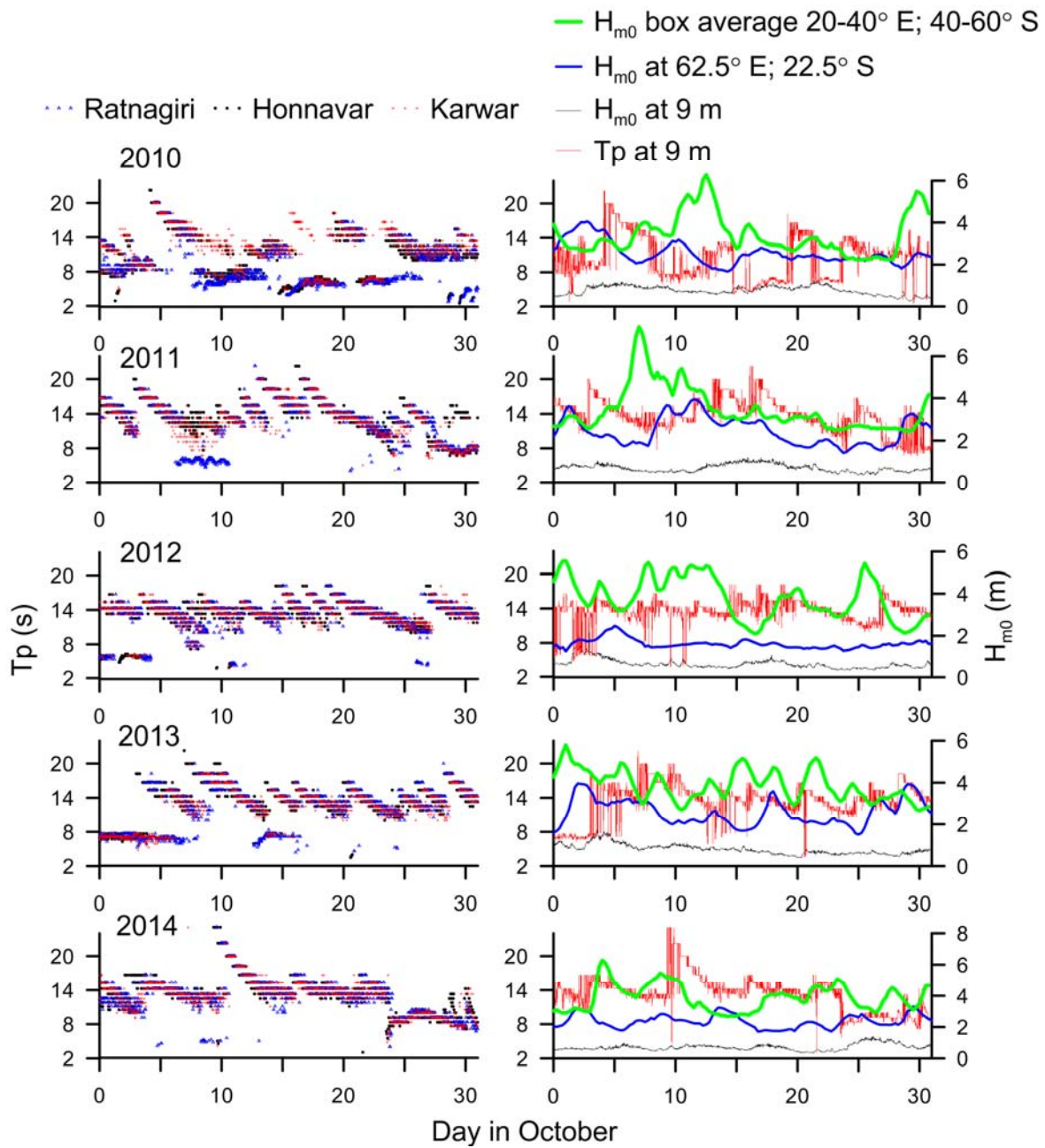


Figure 8.

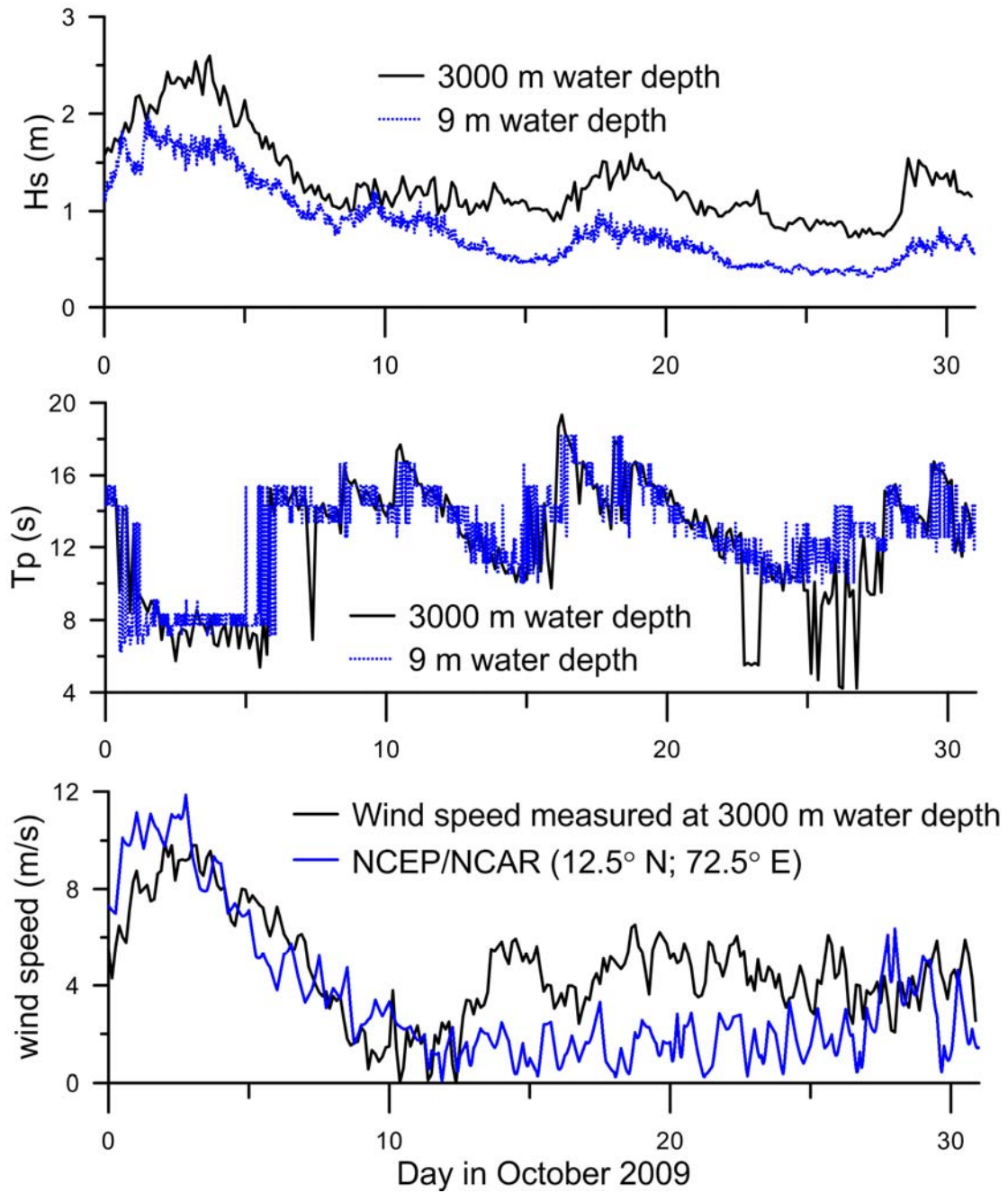


Figure 9.

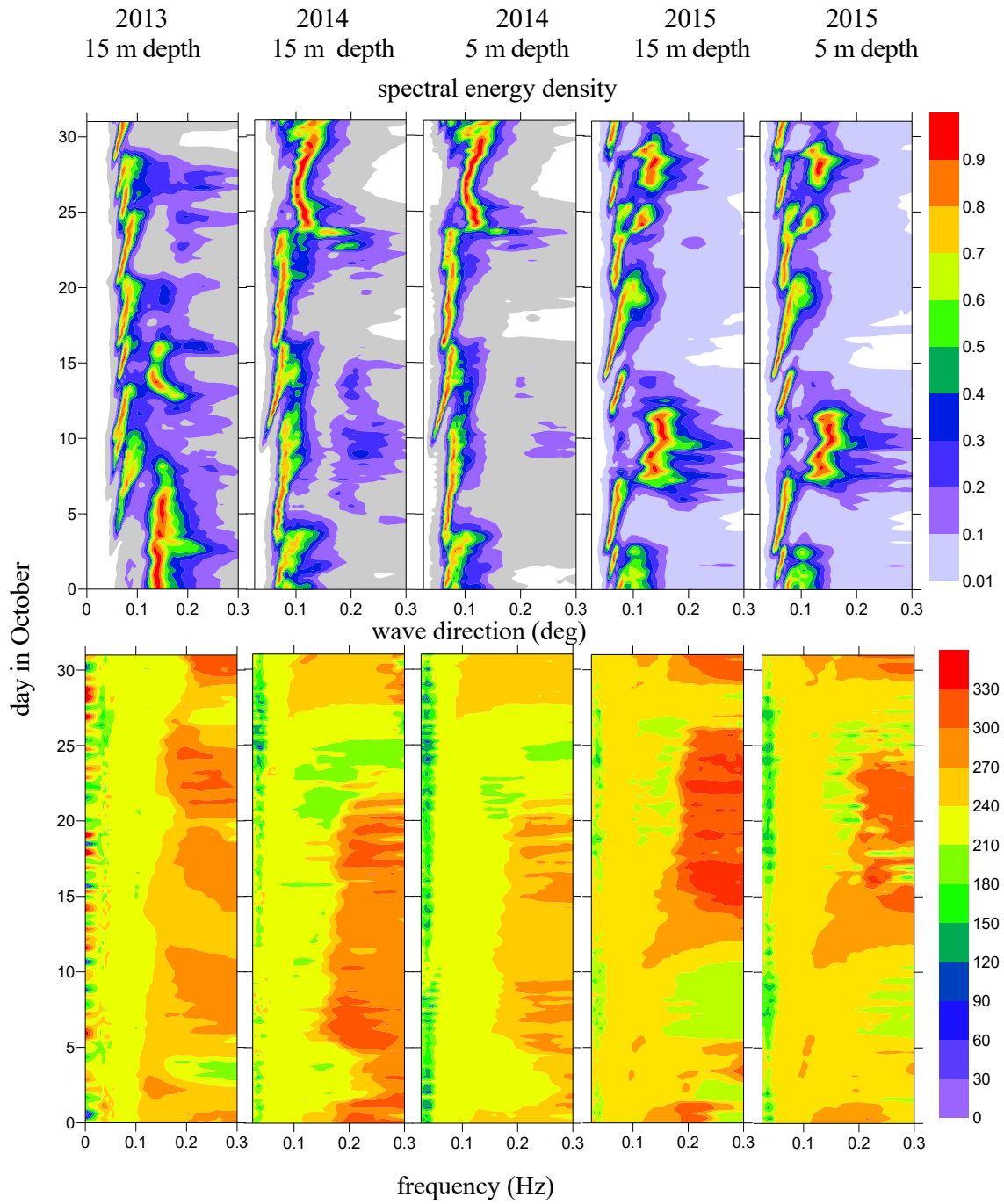


Figure 10.

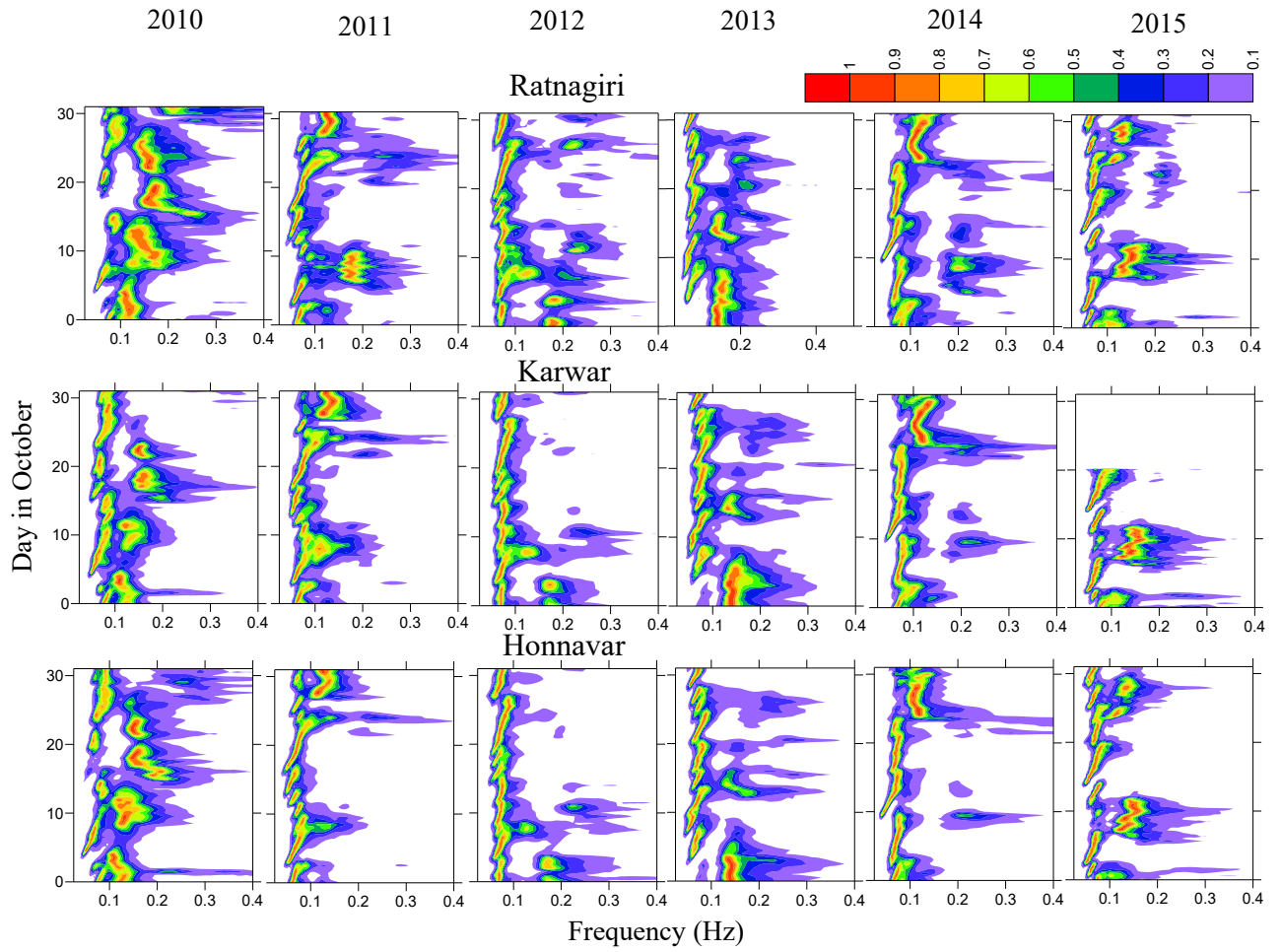


Figure 11.

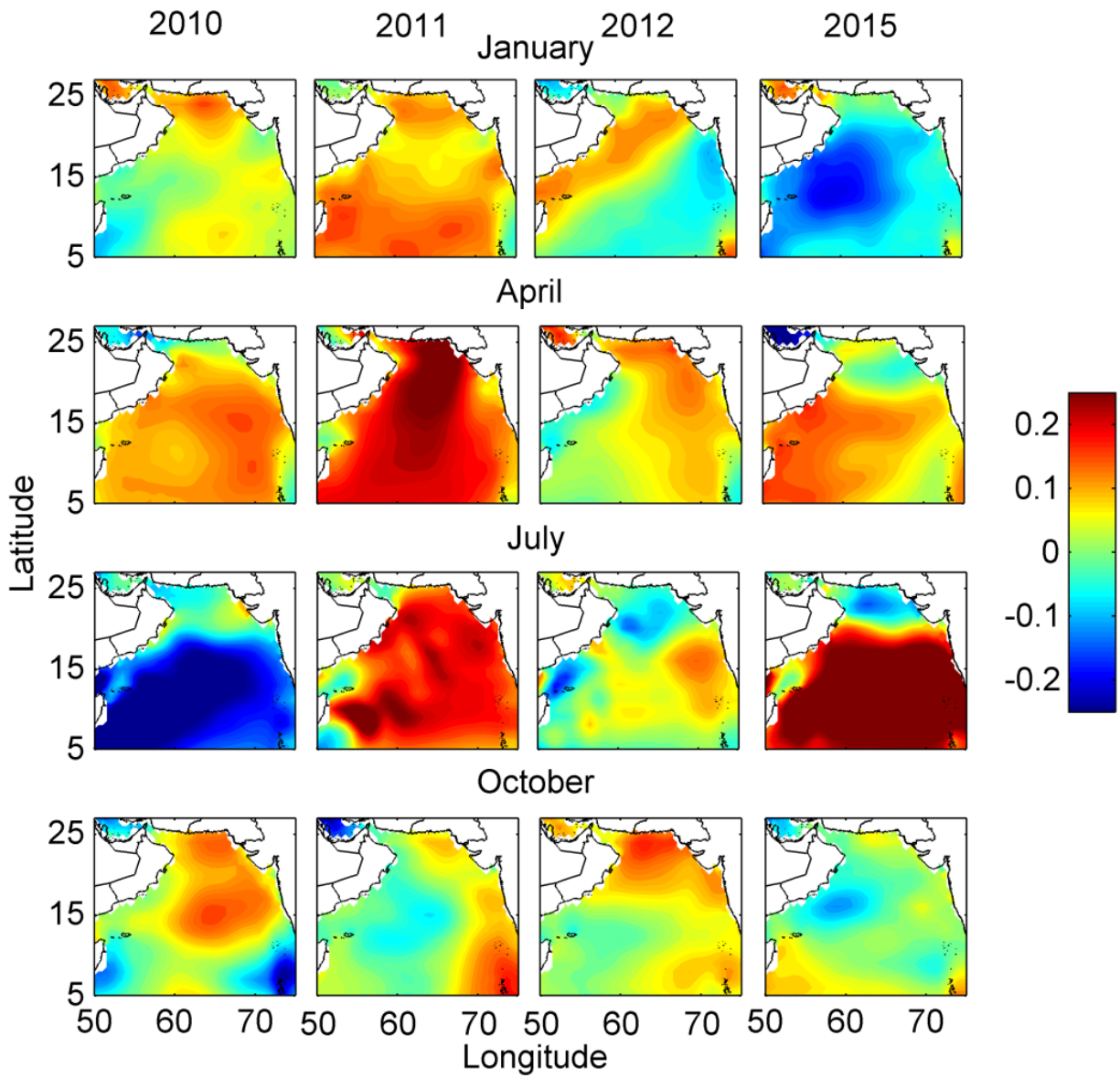


Figure 12.

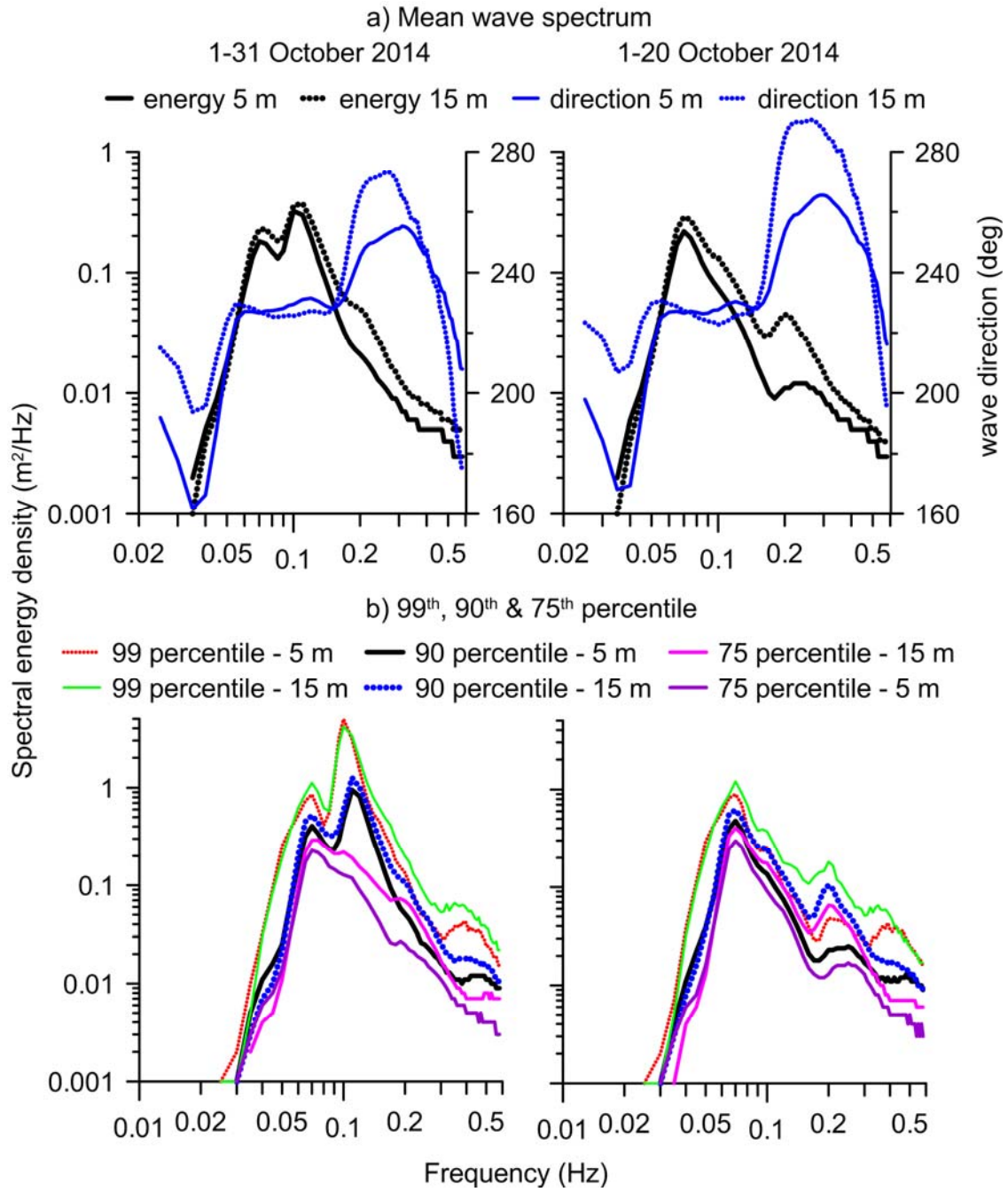


Figure 13. a) b)

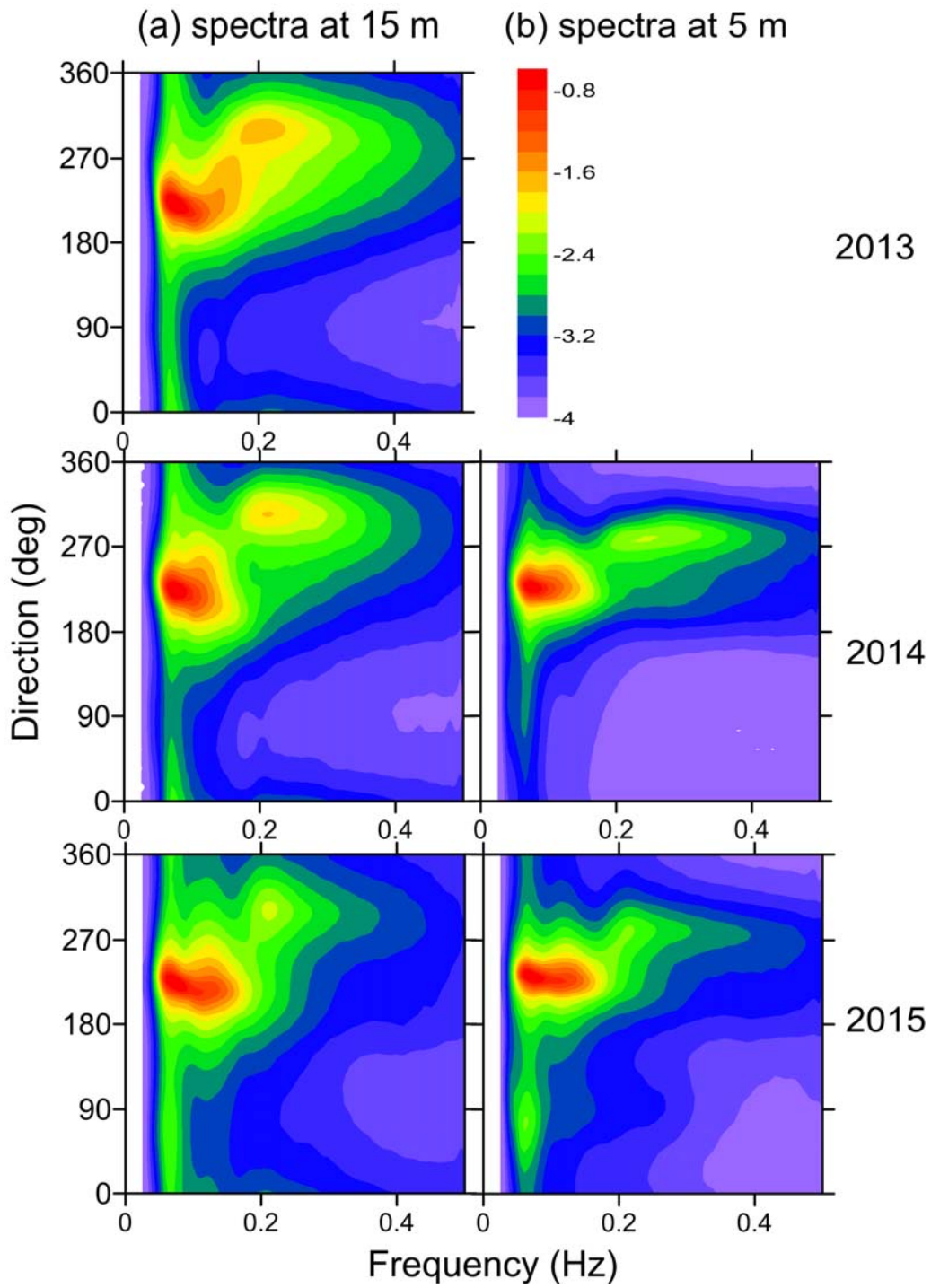


Figure 14.

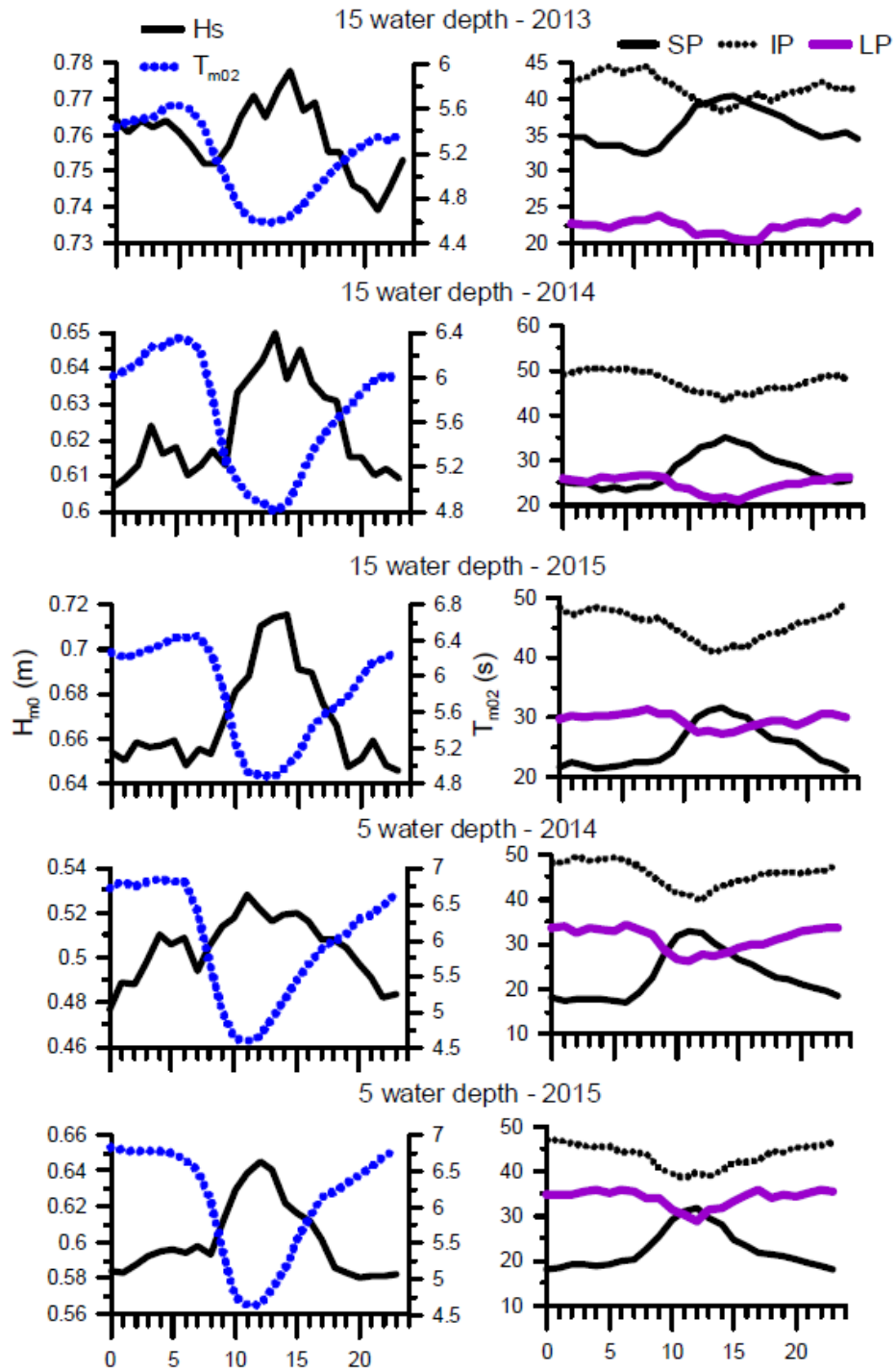


Figure 15.

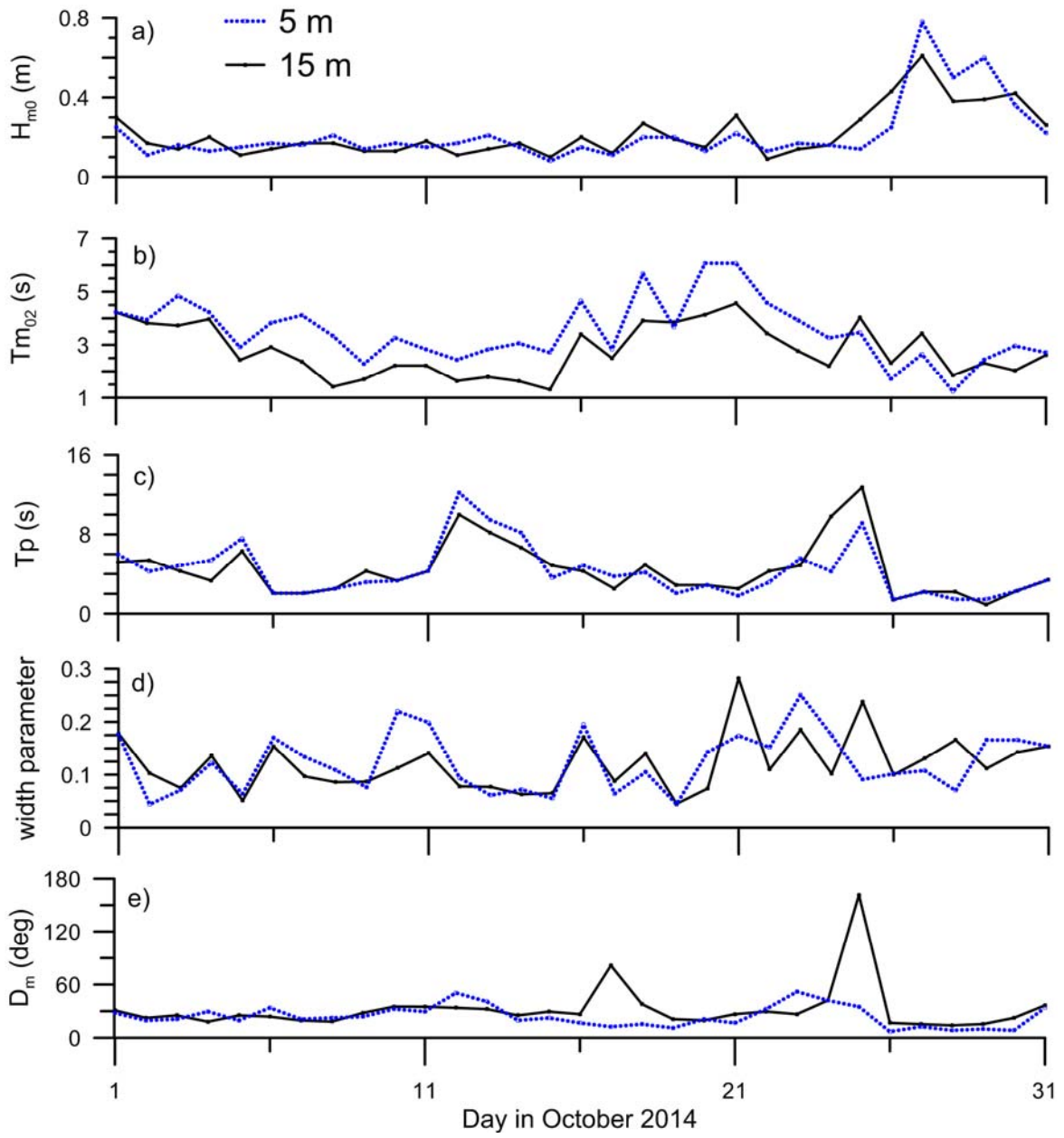


Figure 16.

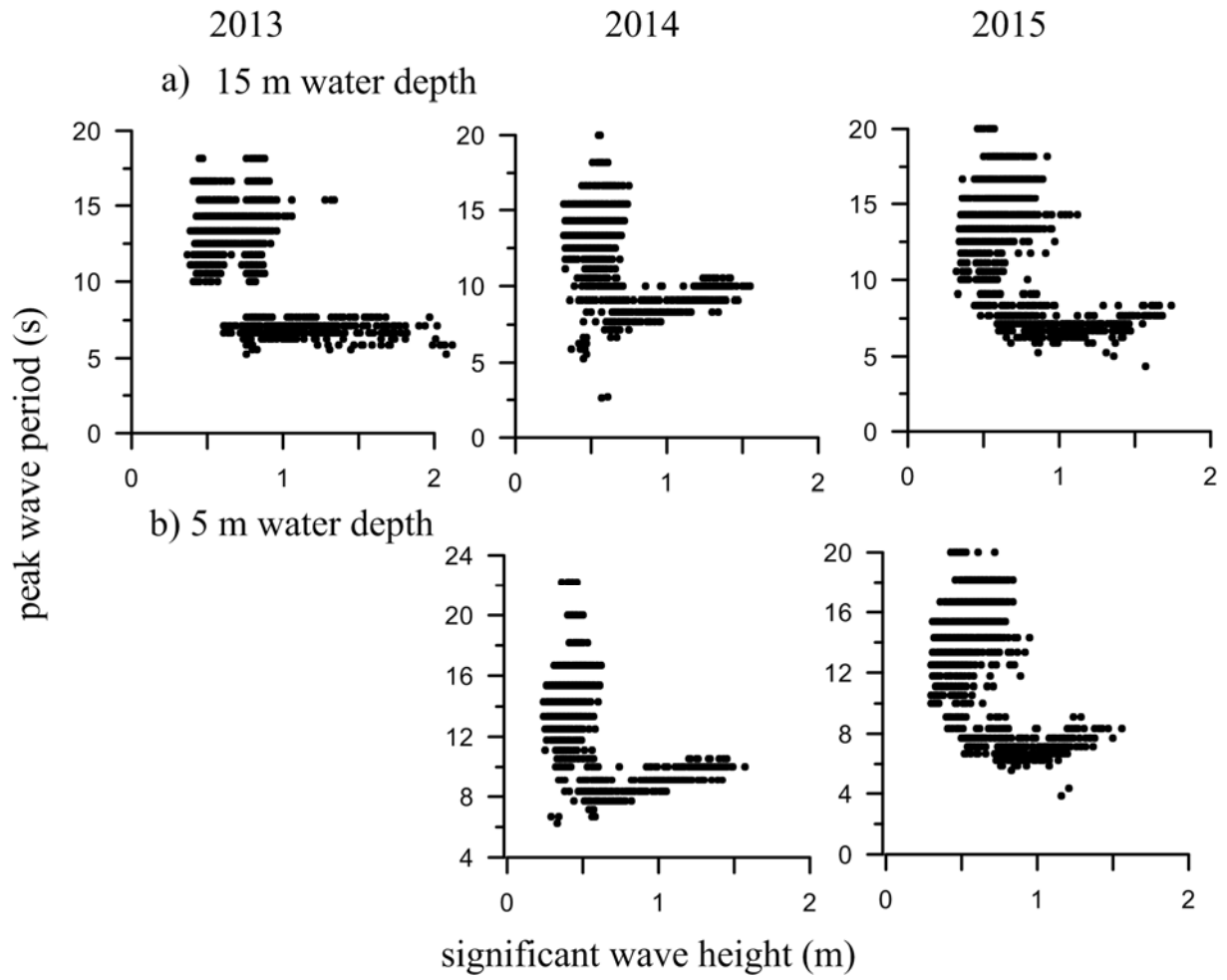


Figure 17.